Check for updates

BASIC SCIENCE ARTICLE

Chemoprevention of bilirubin encephalopathy with a nanoceutical agent

Aniruddha Adhikari[1], Vinod K. Bhutani[2], Susmita Mondal[1], Monojit Das[3,4], Soumendra Darbar[5], Ria Ghosh[6], Nabarun Polley[7], Anjan Kumar Das[8], Siddhartha Sankar Bhattacharya[3], Debasish Pal[3], Asim Kumar Mallick[9] and Samir Kumar Pal[1,3,6 ✉]

BACKGROUND: Targeted rapid degradation of bilirubin has the potential to thwart incipient bilirubin encephalopathy. We investigated a novel spinel-structured citrate-functionalized trimanganese tetroxide nanoparticle (C-Mn_3O_4 NP, the nanodrug) to degrade both systemic and neural bilirubin loads.

METHOD: Severe neonatal unconjugated hyperbilirubinemia (SNH) was induced in neonatal C57BL/6j mice model with phenylhydrazine (PHz) intoxication. Efficiency of the nanodrug on both in vivo bilirubin degradation and amelioration of bilirubin encephalopathy and associated neurobehavioral sequelae were evaluated.

RESULTS: Single oral dose (0.25 mg kg^{-1} bodyweight) of the nanodrug reduced both total serum bilirubin (TSB) and unconjugated bilirubin (UCB) in SNH rodents. Significant ($p < 0.0001$) UCB and TSB-degradation rates were reported within 4–8 h at 1.84 ± 0.26 and 2.19 ± 0.31 mg dL^{-1} h^{-1}, respectively. Neural bilirubin load was decreased by 5.6 nmol g^{-1} ($p = 0.0002$) along with improved measures of neurobehavior, neuromotor movements, learning, and memory. Histopathological studies confirm that the nanodrug prevented neural cell reduction in Purkinje and substantia nigra regions, eosinophilic neurons, spongiosis, and cell shrinkage in SNH brain parenchyma. Brain oxidative status was maintained in nanodrug-treated SNH cohort. Pharmacokinetic data corroborated the bilirubin degradation rate with plasma nanodrug concentrations.

CONCLUSION: This study demonstrates the in vivo capacity of this novel nanodrug to reduce systemic and neural bilirubin load and reverse bilirubin-induced neurotoxicity. Further compilation of a drug-safety-dossier is warranted to translate this novel therapeutic chemopreventive approach to clinical settings.

IMPACT:

- None of the current pharmacotherapeutics treat severe neonatal hyperbilirubinemia (SNH) to prevent risks of neurotoxicity.
- In this preclinical study, a newly investigated nano-formulation, citrate-functionalized Mn_3O_4 nanoparticles (C-Mn_3O_4 NPs), exhibits bilirubin reduction properties in rodents.
- Chemopreventive properties of this nano-formulation demonstrate an efficacious, efficient agent that appears to be safe in these early studies.
- Translation of C-Mn_3O_4 NPs to prospective preclinical and clinical trials in appropriate in vivo models should be explored as a potential novel pharmacotherapy for SNH.

INTRODUCTION

Access to safe, affordable, and effective chemopreventive agents for the clinical crisis of severe neonatal hyperbilirubinemia (SNH) remains an unmet, urgent, and current global health need. A reliable, single intervention strategy could bridge the ongoing fractured maternal child health services in disrupted and dislocated communities.[1–3] The burden of persistent, unmonitored, and untreated SNH in resource-constrained communities is well documented.[4–6] The adverse consequences are well known such that the risk of irreversible life-long brain injury places about 2% of the world's newborn population at jeopardy of both morbidity and mortality.[5–8] Introductions of biologically relevant hemeoxygenase inhibitors, invented at the Rockefeller Institute,[9–12] and supported by US academic (NIH) and corporate

¹Department of Chemical, Biological and Macromolecular Sciences, S. N. Bose National Centre for Basic Sciences, Block JD, Sector 3, Salt Lake, Kolkata 700106, India. ²Department of Neonatal and Developmental Medicine, Lucile Packard Children's Hospital, Stanford University, 750 Welch Road, Palo Alto, CA 94304, USA. ³Department of Zoology, Uluberia College, University of Calcutta, Uluberia, Howrah 711315, India. ⁴Department of Zoology, Vidyasagar University, Rangamati, Midnapore 721102, India. ⁵Research and Development Division, Dey's Medical Stores (Mfg.) Pvt. Ltd., 62 Bondel Road, Ballygunge, Kolkata 700019, India. ⁶Technical Research Centre, S. N. Bose National Centre for Basic Sciences, Block JD, Sector 3, Salt Lake, Kolkata 700106, India. ⁷Physical Chemistry – innoFSPEC, University of Potsdam, Am Mühlenberg 3, Golm, 14476 Potsdam, Germany. ⁸Department of Pathology, Coochbehar Govt. Medical College and Hospital, Silver Jubilee Road, Coochbehar 736101, India. ⁹Department of Pediatric Medicine, Nil Ratan Sirkar Medical College and Hospital, 138 AJC Bose Road, Sealdah, Rajabazar, Kolkata 700014, India. ✉email: skpal@bose.res.in

sponsors (tin-mesoporphyrin[3,10,13]) failed to attain United States Food and Drug Administration (US-FDA) approval.[14]

Recent advances in nano-chemistries, such as applications of nanometer-sized colloidal particles (i.e., nanoparticles), have emerged for their unique tunable electronic, optical, and magnetic properties that are derived from the nanoscale dimensions and compositions.[15–18] In fact, several therapeutic and diagnostic modalities have been reported for a diverse array of nanomaterials.[18–20] Doxil® (doxorubicin liposomes) is one such agent that has been approved by the US-FDA for treatment of AIDS-associated Kaposi's sarcoma.[21] Similarly, Abraxane®, a 130-nm paclitaxel-functionalized albumin, was approved as a second-line drug treatment for breast cancer.[22] Other clinical nano-pharmacotherapeutics include Combidex® (ferumoxtran-10), DexFerrum®, Ferrlecit®, Injectafer®, etc. (comprehensively reviewed in ref.[19]). Engineered multivalent manganese oxide (i.e., Mn_xO_y) nanomaterials were recently considered as therapeutic agents in animal models of hepatic fibrosis,[23] chronic kidney disease[24] as well as neurodegenerative disorders[25–27] and encouraged our inquiry. Manganese (Mn) is an essential trace mineral nutrient and serves as a co-factor for key metabolic enzymes such as superoxide dismutase (SOD), arginase, and pyruvate carboxylase.[28] The bioavailability of Mn is well documented and promoted for its vital role in the metabolism of amino acids, cholesterol, glucose, and carbohydrate; scavenging of reactive oxygen species; bone formation; synthesis of sex hormones, and immune response.[29–32] Additional beneficial properties of nano-doses of manganese include its exciting redox modulatory and catalytic properties for therapeutic applications.[27,33–35] On the other hand, occupational over-exposure to Mn has known adverse events[36,37] and led to designated safe therapeutic thresholds.[38] Prior to embarking on this current study, we demonstrated that citrate-functionalized manganese oxide-nanoparticles (C-Mn$_3$O$_4$ NPs) do not manifest characteristic evidence of Mn-neurotoxicity; rather, Mn-induced neurologic disorder (e.g., idiopathic Parkinson's disorder) was ameliorated through mitochondrial protection and intracellular redox modulation.[26] Biocompatibility and safety of C-Mn$_3$O$_4$ NPs have also been reported.[39] Our preliminary experiments with these nanoparticles were also suggestive of unprecedented catalytic activity toward bilirubin degradation without any photo- or chemo-activation in a controlled in vitro system.[40]

For this current study, we designed a cohort of two-phased experiments to examine the processes and mechanisms for bilirubin degradation by C-Mn$_3$O$_4$ NPs (the nanodrug) in a proven rodent model specifically bred to manifest SNH and associated neurotoxicity. Each set of cohorts comprised: (i) primary control of healthy rodents, (ii) control SNH model with phenylhydrazine (PHz)-induced SNH (kernicteric model in the second phase), (iii) SNH model treated with the chosen nanodrug as the specific experimental model (kernicteric model treated with the nanodrug), and (iv) another control cohort of healthy rodents treated with nanodrug alone. Our primary outcome measures were (a) to determine both systemic and neural bilirubin degradation; (b) effect on neuromotor function and neurobehavioral abilities of survivors in the kernicteric model; and (c) the pharmacokinetics and dynamics of the nanodrug.

METHODS
Rodent model
To evaluate the in vivo effectiveness of the nanodrug in degradation of bilirubin, we developed a chemical (i.e., PHz) induced mice model that closely resembles the pathophysiological condition of human neonatal jaundice characterized by high systemic unconjugated bilirubin (UCB) due to higher hemoglobin (Hb) turnover, shorter red blood cell lifespan and inability of developing liver to efficiently eliminate or conjugate bilirubin.[41,42]

All animal studies and experimental procedures were performed at Central Animal Facility, Department of Zoology, Uluberia College, India (Reg. No.: 2057/GO/ReRcBi/S/19/CPCSEA) following the protocol approved by the Institutional Animal Ethics Committee (Ref: 02/S/UC-IAEC/01/2019). Non-diabetic infant C57BL/6j mice of both sexes (age: 6 days, BW: 7.1 ± 0.9 g) were used. For detailed methods see the Supplementary Methods section.

Induction of SNH
PHz-intoxication induced drastic catabolism of the circulating Hb to accumulated bilirubin and lead to SNH by hemolysis without hepatic involvement.[42–44] To minimize the potential impact of UDP-glucuronosyltransferases (UGT1) maturation on bilirubin clearance, we completed our studies within postnatal day 14 as prior studies suggested the expression of UGT1 in mice commences at postnatal age 14 days.[6,45]

Randomization and dosing
Mice were randomly divided into four cohorts (Phase I study): (i) healthy control ($n = 20$): healthy control received a placebo, normal saline (150 μL, po); (ii) SNH model ($n = 30$): SNH model received three doses of PHz (30 mg kg^{-1} BW, i.p.) at postnatal ages 6, 8 and 10 days; (iii) nanodrug treated ($n = 30$): the experimental cohort of SNH model treated with nanodrug, received C-Mn$_3$O$_4$ NPs (0.25 mg kg^{-1} BW; po) at postnatal age 10 days; (iv) nanodrug control ($n = 20$): healthy rodent cohort treated with the nanodrug, C-Mn$_3$O$_4$ NPs (0.25 mg kg^{-1} BW; oral) alone as the non-SNH model at postnatal age 10 days. All primary outcomes were evaluated at age 10 days.

To assess the effect on bilirubin neurotoxicity, a kernicterus-like syndrome, a series of experiments were designed on four rodent cohorts (Phase II study) randomized to: (i) healthy control ($n = 20$): healthy controls treated with an oral saline placebo (150 μL; po); (ii) SNH model ($n = 30$): SNH model administered with three serial doses of PHz (30 mg kg^{-1} BW, i.p.) at postnatal ages 6, 8 and 10 days; (iii) nanodrug treated ($n = 30$): SNH model serially treated with C-Mn$_3$O$_4$ NPs (0.25 mg kg^{-1} BW; po) at postnatal ages 6, 8, 10 and 12 days; (iv) nanodrug control ($n = 20$): healthy cohort solely treated with C-Mn$_3$O$_4$ NPs (0.25 mg kg^{-1} BW; po) at postnatal ages 8, 10, and 12 days. Brain samples ($n = 10$) were collected from each group on day 13. All neurobehavioral studies were performed in the remainder cohorts between postnatal days 14 and 18. Supplementary Table 1 outlines the timeline of the phased experiments.

Serum bilirubin assay
Blood samples were collected from retro-orbital-plexus and serum was instantly separated by centrifugation at 4 °C, in dark. Total serum bilirubin (TSB), and UCB were measured following di-azo method using commercially available test kits (Autospan Liquid Gold, Span Diagnostic Ltd., India).

Brain gross anatomy
The gross anatomy of the brain was studied immediately after excision at the postnatal age of 14 days. The brains were photographed using a digital camera in the manual mode keeping all the instrumental parameters the same across groups. The deposition of bilirubin was calculated by counting yellow pixel density in Photoshop 2022 (Adobe Inc.).

Brain histopathology
For histopathological investigation, brains were removed from the sacrificed animals, and fixed in 10% buffered formalin for 7 days. Paraffin-embedded sections (5–8 μm) were stained with hematoxylin and eosin following the standard method.

Neural bilirubin loads (post-mortem)
Gross neural bilirubin loads were measured using a previously published protocol.[46] Briefly, the brain sections were homogenized, and bilirubin was extracted using an organic extraction solvent: methanol/chloroform/n-hexane (63:31:6, v/v) and measured using a spectrophotometer (Model UV-Vis 2600, Shimadzu, Japan) at 420 nm.

Brain oxidative status
Extent of lipid peroxidation (i.e., malonyldialdehyde (MDA) level) was determined in the brain homogenates according to Buege methodology.[47] The activity of SOD, catalase (CAT), glutathione peroxidase (GPx), glutathione-disulfide (GSSG), and reduced glutathione (GSH) were estimated using commercially available test kits (Sigma-Aldrich, MO).

Distribution in the brain

Mn-contents in the brain (12 h after po administration of nanodrug) were assayed by inductively coupled plasma atomic emission spectroscopy (ICP-AES) (ARCOS-Simultaneous ICP Spectrometer, SPECTRO Analytical Instruments, Germany). Open acid-digestion method was used during the sample preparation.[48]

Neuromotor function analysis (survivors)

The neuromotor functions were evaluated using four tests: (i) open field test (OFT) for measurements of spontaneous activity; (ii) balance beam test for fine motor control; (iii) pole test for motor coordination; and (iv) gait analysis for movement pattern. See Supplementary Methods for details.

Cognitive function test

To assess hippocampus-dependent learning and memory, we used two variants of well-known Morris water maze (MWM) test: (i) the hidden platform test, and (ii) cue reversal test. Furthermore, we performed novel object recognition (NOR) test to assess recognition memory. See Supplementary Methods for details.

Pharmacokinetics and dynamics (PK-PD) studies

For PK-PD analysis a separate group of 36 animals were induced SNH with three doses of PHz (30 mg kg^{-1} BW, i.p.) at postnatal ages 6, 8, and 10 days and then treated with the nanodrug (0.25 mg kg^{-1} BW, po at postnatal day 10) and were sampled at 0, 0.5, 1, 2, 4, 6, 8, 12, and 24 h ($n = 4$ each time). Mn-contents were assayed by ICP-AES.

Statistical analysis

All quantitative data are expressed as mean ± standard deviation, unless otherwise stated. Unpaired t-test with Welch's correction was used to compare between two groups. One-way analysis of variance followed by correction of false discovery rate (post hoc FDR: two-stage step-up method of Benjamini et al.[49]) for multiple comparisons was performed for comparison between multiple groups. Designated sample size always refers to biological replicates (independent animals). GraphPad Prism v8.0 (GraphPad Software), and Sigmaplot v14.0 (Systat Software, Inc.) were used for statistical analysis. For all comparisons, a p value < 0.05 was considered statistically significant.

RESULTS

Bilirubin loads in blood chemistry for the chemically induced C57BL/6j mice model (Fig. 1a) depicts significantly elevated ($p < 0.0001$) systemic UCB: (8.58 ± 0.37 mg dL^{-1}) and TSB (11.04 ± 1.01 mg dL^{-1}) at postnatal age 10 days compared with the similar aged healthy control littermates (UCB: 0.32 ± 0.02 mg dL^{-1}; TSB: 0.45 ± 0.09 mg dL^{-1}). Single oral nanodrug (0.25 mg kg^{-1} BW) to the SNH mice at postnatal age 10 days, irreversibly decreased both UCB (0.74 ± 0.19 mg dL^{-1}; $t(6.07) = 43.07$, $p < 0.0001$) and TSB (1.69 ± 0.14 mg dL^{-1}; $t(4.31) = 28.46$, $p < 0.0001$) to normal range within 12 h (Fig. 1a–c). Logistic regression of the UCB-degradation kinetic data (adj. R^2 0.997) revealed the time required for degrading 50% and 80% bilirubin to be 6.07 ± 0.08 h and 7.44 ± 0.17 h, respectively. Similarly for TSB the times required were 6.47 ± 0.18 h and 8.05 ± 0.37 h (adj. R^2 0.990). The sequential rates of bilirubin degradation are illustrated in Fig. 1 (insets b and c) that show significant UCB- and TSB-degradation rates consequent to the nanodrug as compared to other control groups during the 4 to 8 h post-administration interval at 1.84 ± 0.26 mg dL^{-1} h^{-1} (~20% h^{-1}) and 2.19 ± 0.31 mg dL^{-1} h^{-1} (~18% h^{-1}), respectively.

Data for the model with kernicterus-like syndrome, induced by repeated and prolonged PHz administration are illustrated in Fig. 2. Here, the "kernicteric" SNH model showed severely elevated bilirubin levels (UCB: 12.3 ± 1.8 mg dL^{-1}, compared to 0.2 ± 0.1 mg dL^{-1} of control littermates; F (3, 18.3) = 134.2, $p < 0.001$; TSB: 14.4 ± 2.4 mg dL^{-1} compared to 0.3 ± 0.1 mg dL^{-1} of control littermates; F (3, 18.3) = 104.0, $p < 0.001$) (Fig. 2a). Physical examination revealed signs of central nervous system (CNS) toxicity as indicated by characteristic seizure patterns and inability

to maintain balance. Deposition of bilirubin in the brain tissue was measured at 7.4 ± 1.2 nmol g^{-1} compared to 0.9 ± 0.5 nmol g^{-1} of control littermates (F (3, 7.7) = 48.6, $p < 0.0001$) (Fig. 2b). Digital photographs (Fig. 2c) clearly depict the intense yellow pigmentation (of bilirubin) in the brain isolated from SNH model cohort as compared to others. Treatment with the nanodrug in the SNH model resulted in decrease in both systemic and neural bilirubin loads (Fig. 2a–c). These observations were evident in the histopathological studies of isolated brain sections (Fig. 2d). Neural damage as quantified by the number of neural cells per field was noticeably reduced in cerebellum (~35%), Purkinje (~30%), and substantia nigra (~40%) in SNH model. Other pathological features of neurotoxicity in the brain micrographs of SNH model included extensive spongiosis (vacuolation linked to depletion of neurons), shrinkage in cell size, eosinophilic neurons (characteristic of degenerating cells), and gliosis. In contrast, the nanodrug-treated model showed normal cellular architecture with mild gliosis, a residual of SNH-induced brain damage (Fig. 2d). The number of cells per field in both cerebellum and midbrain region was comparable to control animals. No shrinkage of cells was observed. Nanodrug control cohort showed normal brain architecture.

Figure 3 illustrates the bilirubin-induced oxidative damages in the cerebellum. In SNH model, unlike the other three cohorts, the cerebellar GSH pool was greatly reduced (7.9 ± 2.4 nmol mg^{-1} protein, compared to 21.4 ± 3.7 nmol mg^{-1} protein of healthy control; F (3, 15.1) = 36.3, $p < 0.001$) (Fig. 3a), and the redox balance was shifted toward oxidative distress (GSH:GSSG ratio: 0.5 ± 0.1, compared to 5.1 ± 0.4 of healthy control; F (3, 12.1) = 100.4, $p < 0.001$) (Fig. 3b). Consequently, lipid peroxidation was significantly higher (MDA content: 26.0 ± 3.5 nmol g^{-1} tissue, compared to 10.7 ± 1.6 nmol g^{-1} tissue of healthy control; F (3, 13.3) = 53.1, $p < 0.001$) in the SNH model (Fig. 3c). Among the three major antioxidant enzymes that regulate the redox status of cerebellar tissue, activity of CAT and GPx were reduced in the SNH model (Fig. 3d, e). No discernable effect on SOD activity was observed among the groups (Fig. 3f). Brain Mn content determined by the ICP-AES provided direct evidence of the presence of the nanodrug in the brain (2.3 ± 0.5 µg g^{-1} tissue in nanodrug treated cohort compared to 0.7 ± 0.1 µg g^{-1} tissue in SNH model; $t(5.39) = 7.68$, $p = 0.0004$).

Representative movement patterns of the rodents in the OFT are shown in Fig. 4a. Decreased spontaneous activity (i.e., total distance moved; Fig. 4b) and increased anxiety parameters (i.e., time spent in the central zone; Fig. 4c) confirmed "long-term" neuralgic sequelae, i.e., motor function and ataxia in SNH model. Higher time to cross the beam (Fig. 4d) and to descend the pole (Fig. 4e) indicates obvious motor-coordination impairment, a prominent signature of bilirubin neurotoxicity. In the gait analysis the SNH model cohorts showed irregular movement patterns (Fig. 4f) with decreased stride length (Fig. 4g), sway length (Fig. 4h), stance angle (Fig. 4i), and stance length (Fig. 4j). No differences between healthy control and nanodrug treated cohorts were found in any of the tests except time to cross the pole ($p = 0.0002$). The Hb-levels were within the normal range and similar for both control and experimental models at the time of behavior studies (data not shown) ruling out the possible effect of anemia in the observed motor functions.

Swimming patterns of different cohorts for the MWM as a measure of hippocampus-dependent learning and memory are shown in Fig. 5a and characterized by known adult swimming features of mice. The times taken to escape from the water during four successive trials are listed in Fig. 5b. All animals except the SNH model cohort learned to escape rapidly from water with stable terminal acquisition latencies of <40s ($p < 0.0001$). The place navigation was further impaired during the platform reversal task (postnatal days 14 and 15). The number of times that SNH model cohort crossed the platform location at postnatal age of 12 days

a UCB and TSB levels before (time 0 h) and 12 hours (time 12 h) after nanodrug administration at postnatal age 10 days

	UCB (mg dL^{-1})			TSB (mg dL^{-1})		
	Time 0 h	Time 12 h	*P*value	Time 0 h	Time 12 h	*P*value
Healthy control	0.32 ± 0.02	0.34 ± 0.04	0.307	0.45 ± 0.09	0.43 ± 0.06	0.662
SNH model	8.45 ± 0.29	8.21 ± 0.38	0.249	11.04 ± 1.01	10.69 ± 0.98	0.556
Nanodrug treated	8.58 ± 0.36	0.74 ± 0.19	<0.0001	10.90 ± 0.71	1.69 ± 0.14	<0.0001
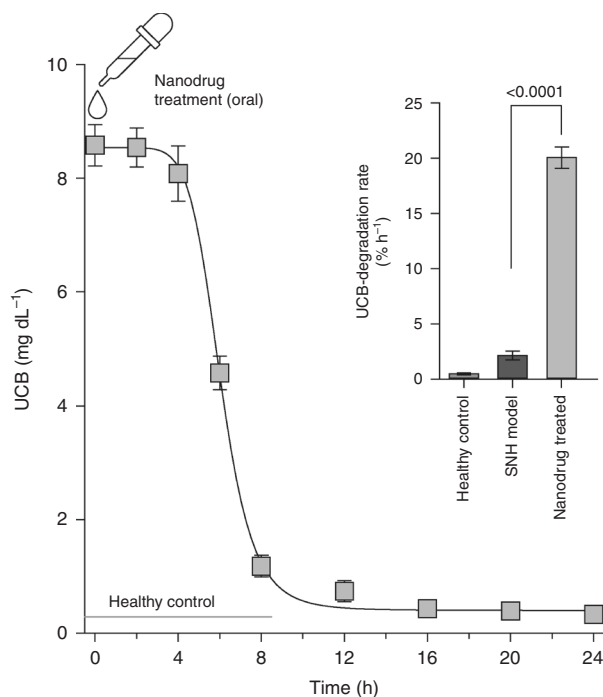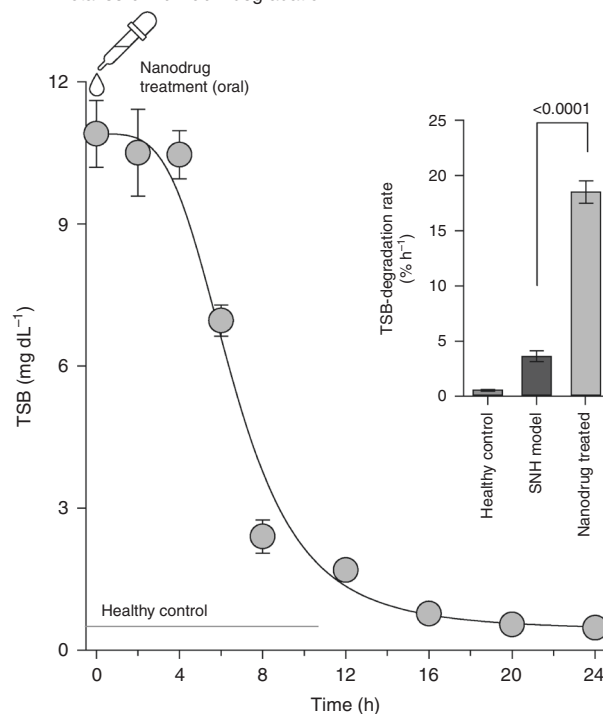
Fig. 1 In vivo bilirubin degradation efficacy of C-Mn$_3$O$_4$ NPs nanodrug in SNH model (postnatal age 10 days). a Tabular representation of UCB and TSB levels before and after nanodrug administration. **b** Time-dependent UCB-degradation kinetics after a single oral dose of nanodrug (0.25 mg kg^{-1} BW). Inset shows percent UCB-degradation rate during 4–8 h post administration. **c** Time-dependent TSB-degradation kinetics after a single oral dose of nanodrug (0.25 mg kg^{-1} BW). Inset shows percent TSB-degradation rate during 4–8 h post administration. Data are expressed as mean ± SD ($n = 6$). One-way ANOVA followed by FDR post hoc multiple comparison test was performed for comparison among the groups.

was distinctly different than that of both healthy control and nanodrug-treated group (Fig. 5c). The SNH model cohort spent significantly less time in the target quadrant (Fig. 5d). In the cued platform reversal test (Fig. 5e) all mice except the SNH model cohort showed a preference for the relative position over the absolute position of the platform, which resulted into "resultant heading error" of ~−75° for SNH model and ~−5° for others ($p < 0.0001$) (Fig. 5f). Retention memory was also impaired in SNH model as they showed a strong preference for neither relative nor absolute platform positioning resulting in the observed scattered directionality across the maze (Fig. 5f). All studied impairments were reversed in the nanodrug-treated cohort.

Data for recognition memory assessed by the NOR task (Fig. 5g) are presented in Fig. 5h–j. As expected, the control mice with fully intact recall memory, spent more time with the novel object than the familiar one (Fig. 5h). In contrast, however, SNH model cohort showed no discrimination ($p = 0.502$) between the novel and familiar objects (Fig. 5h). Thus, the preference index (Fig. 5i) and discrimination ability (Fig. 5j) were both impaired in the SNH model. Treatment with nanodrug reversed these profound

cognitive-deficits and the animals behaved like the healthy control cohort (Fig. 5h–j).

Pharmacokinetics and pharmacodynamics are shown in Fig. 6. Time-dependent plasma concentration profiles of the nanodrug after po delivery are presented as plasma Mn-concentration versus time plot. The PK parameters were calculated for a non-compartmental approach and presented in Fig. 6. The mean plasma concentration curve presented three-peak absorption phases at ~1.0, ~6.0, and 12.0 h (Fig. 6a). The deconvoluted spectra show a significant overlap between intestinal absorption and hepato-biliary reabsorption, which resulted in the higher third peak (~12 h). The first peak may be due to the absorption in the upper gastrointestinal tract, as direct delivery of the nanodrug to the stomach by oral gavage resulted in the disappearance of the first peak (Fig. 6c). Urinary Mn levels were below the detectable range. Mn content of feces have maximum concentration ($C_{MAX} = 0.68 ± 0.07$ µg g^{-1}) at ~18.0 h (Fig. 6b). The effect of the nanodrug on bilirubin degradation correlated with plasma nanodrug-concentration profile (Fig. 6d) with an inverse relationship. Figure 6e describes a dose-dependent correlation (adj. R^2
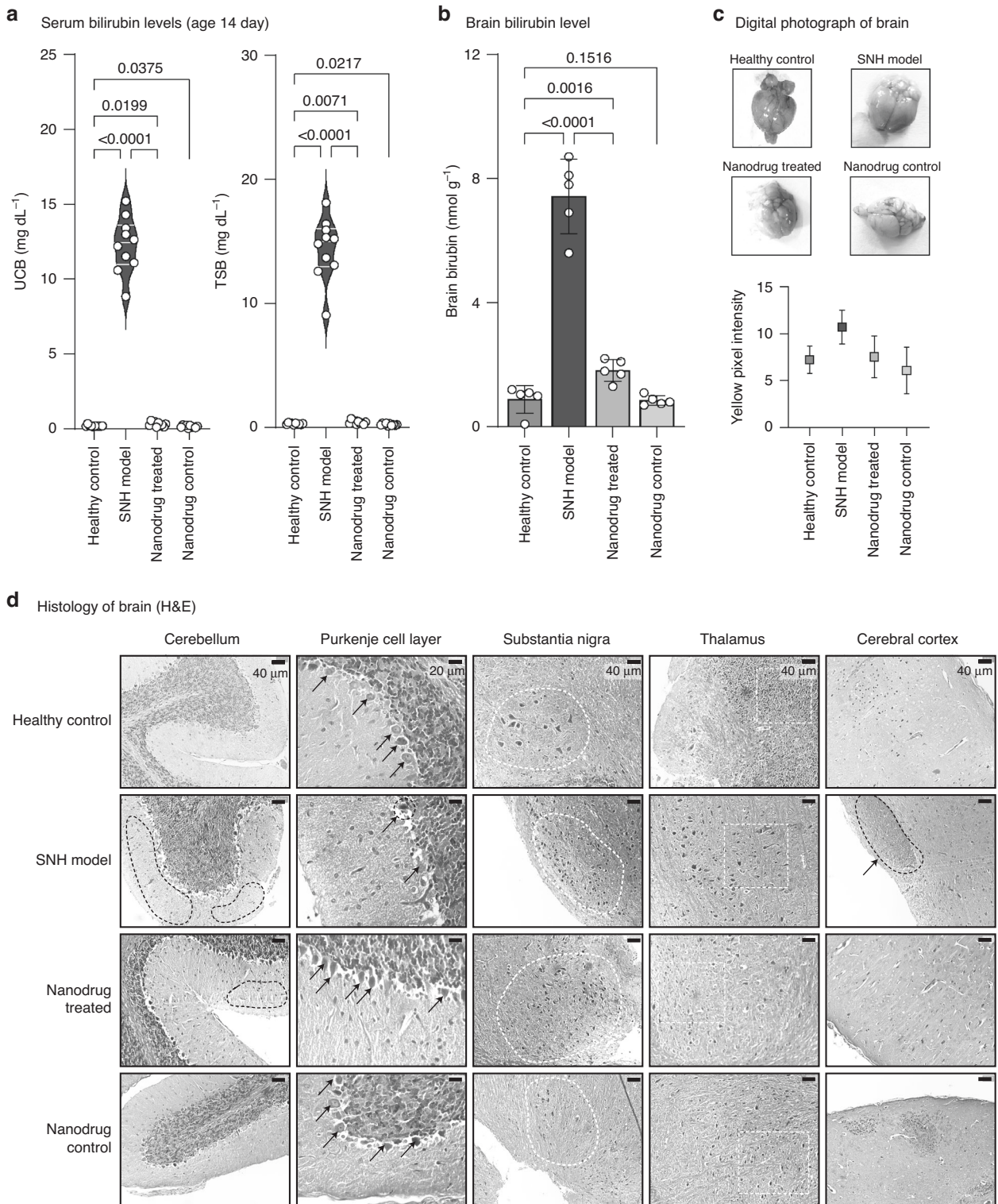
Fig. 2 Effect of the nanodrug on prevention of SNH-associated neurotoxicity. a UCB and TSB levels on postnatal age 14 days. **b** Brain bilirubin load. **c** Representative digital micrographs of brains and quantification of yellow color intensity. The intense yellow discoloration of the brain from SNH model cohort in comparison to the other cohorts must be noted. **d** Micrographs of hematoxylin and eosin (H&E)-stained histopathological sections of different brain regions. The dotted areas indicate the regions of interest where degenerative changes like reduction in neural cells numbers, spongiosis, shrinkage in cell size and eosinophilic neurons took place. The black arrows indicate the Purkinje cells, whose density is greatly reduced in SNH model. In bar plots, data are expressed as mean ± SD ($n = 6$). Violins depict kernel density estimation of the underlying data distribution. Three lines (from the bottom to the top) in each violin plot show the location of the lower quartile (25th), the median, and the upper quartile (75th), respectively. Individual data points are represented as colored circles or squares ($n = 10$). One-way analysis of variance (ANOVA) followed by FDR post hoc multiple comparison test was performed for comparison among the groups.
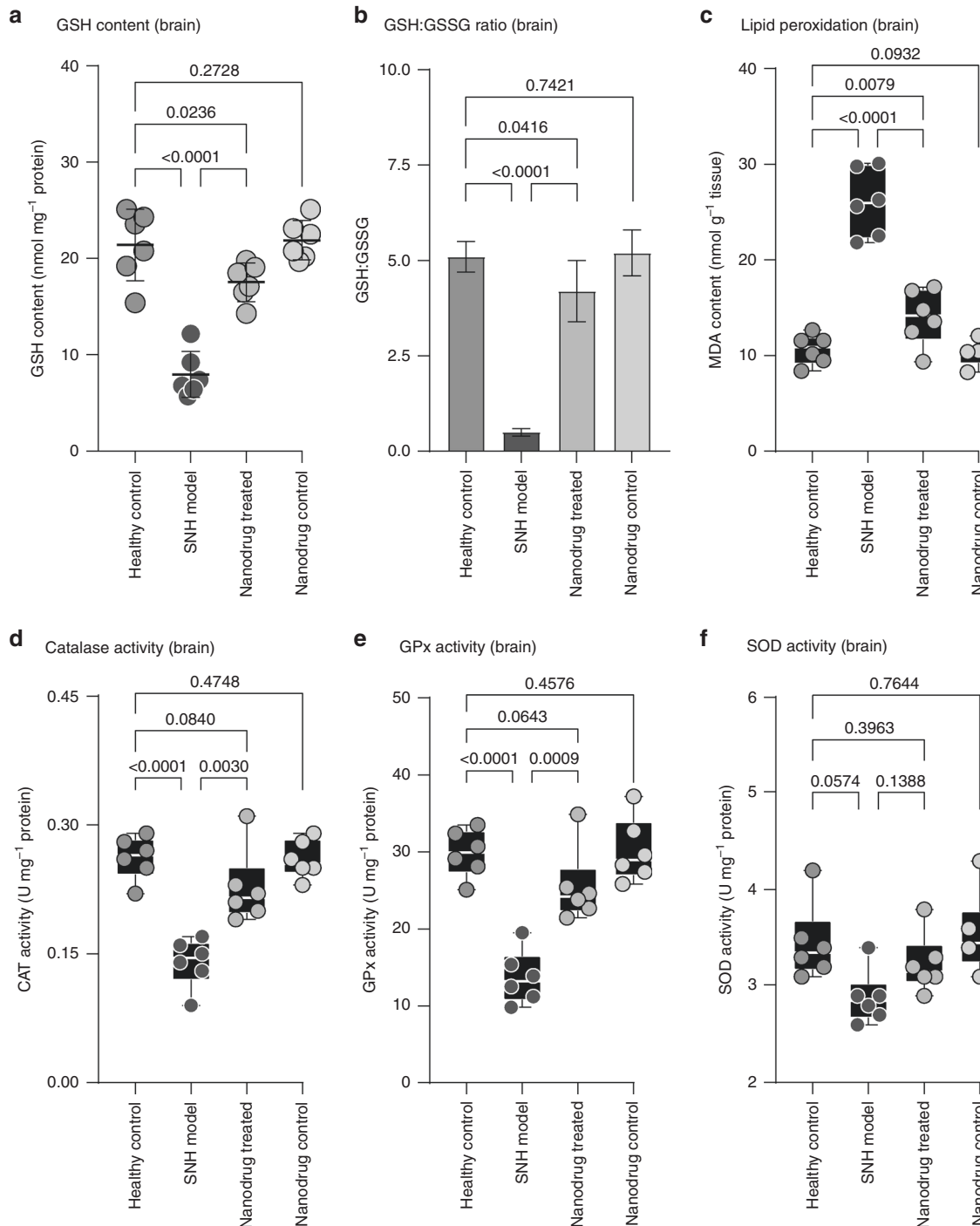
Fig. 3 Effect of the nanodrug on SNH-associated brain (cerebellar) oxidative distress. a Reduced glutathione (GSH) content. **b** Ratio of reduced and oxidized glutathione (GSH:GSSG). **c** Lipid peroxidation. **d** Catalase (CAT) activity. **e** Glutathione peroxidase (GPx) activity. **f** Superoxide dismutase (SOD) activity. In bar plots data are expressed as mean ± SD ($n = 6$). Box plot shows lower quartile (25th), the median, the upper quartile (75th), and range of data points. Individual data points are represented as colored circles ($n = 6$). One-way analysis of variance (ANOVA) followed by FDR post hoc multiple comparison test was performed for comparison among the groups.

0.995; non-linear logistic-regression model) suggestive of in vivo catalytic degradation of bilirubin by the nanodrug.

DISCUSSION
We report a novel chemopreventive nanoceutical agent, C-Mn₃O₄ NPs (the nanodrug), that has the capacity to selectively degrade bilirubin in vivo and unique properties to reverse acute bilirubin neurotoxicity.

We provide direct evidence for a single oral dose of the nanodrug to degrade UCB, both systemic and neural. Significant ($p < 0.0001$) UCB and TSB-degradation rates were reported within 4–8 h at 1.84 ± 0.26 mg dL^{-1} h^{-1} (~20% h^{-1}) and 2.19 ± 0.31 mg dL^{-1} h^{-1} (~18% h^{-1}) as compared to control cohorts, respectively. In the long-term SNH with kernicterus-like syndrome model, brain bilirubin load was decreased by 5.6 nmol g^{-1} ($p = 0.0002$) along with improved neurobehavior, neuromotor movements as well as hippocampus-

Gross locomotor activity
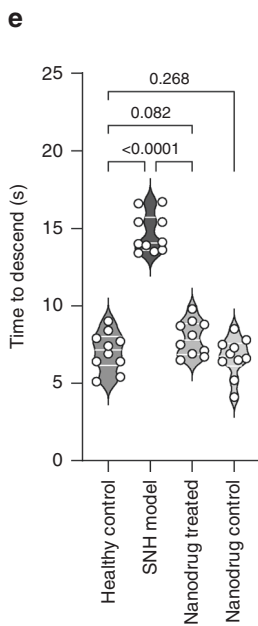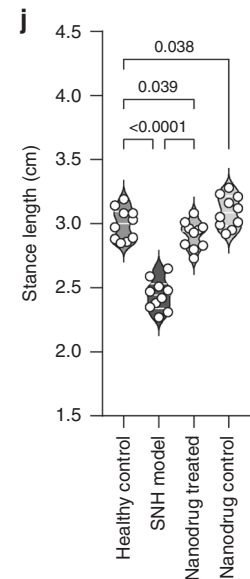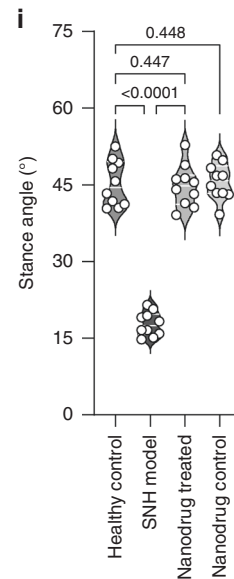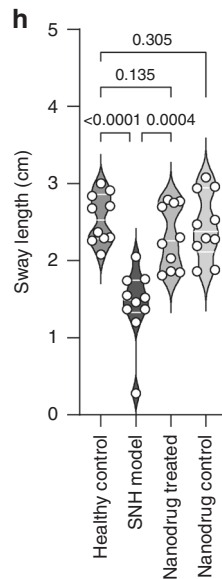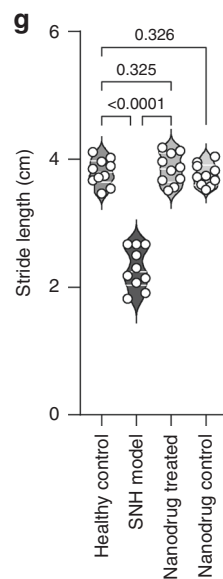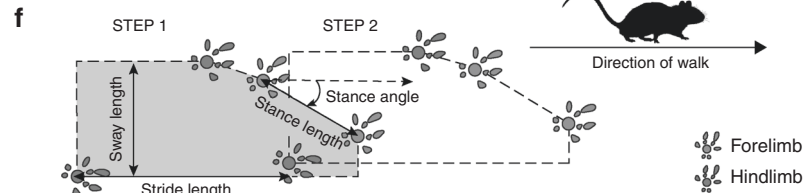Open-field test (OFT)
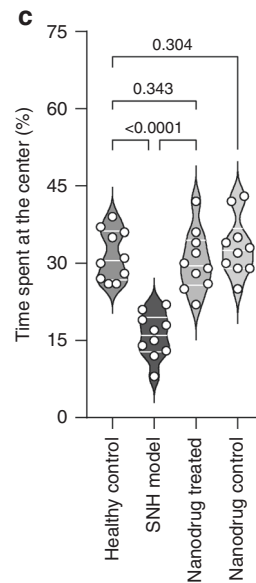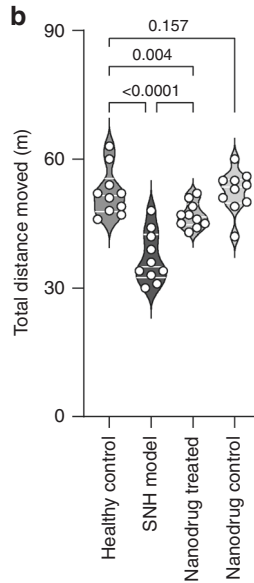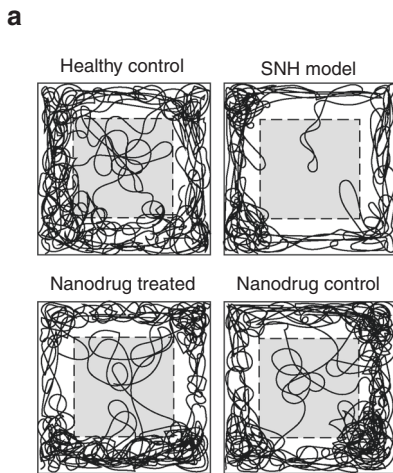
**Fine motor function**
Beam travesel test
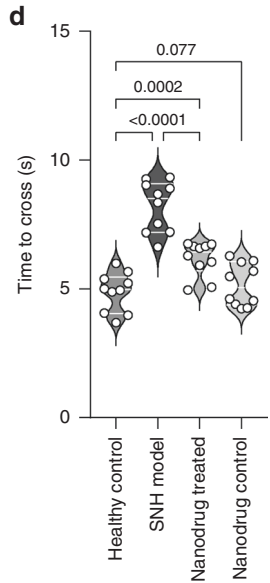
Fine motor function
Pole test

Gait analysis

Fig. 4 Effect of the nanodrug on SNH-associated neuromotor function. Open field test (OFT): **a** Movement pattern of the rodents in the open field. **b** Total distance moved. **c** Times spent in the central region. Beam Traversal Test: **d** Time to cross the beam. Pole Test: **e** Time to descend the pole. Gait Analysis: **f** General gait pattern of rodents and different parameters used for quality assessment of the movement. **g** Stride length. **h** Sway length. **i** Stance angle. **j** Stance length. Violins depict kernel density estimation of the underlying data distribution. Three lines (from the bottom to the top) in each violin plot show the location of the lower quartile (25th), the median, and the upper quartile (75th), respectively. Individual data points are represented as white circles ($n = 10$). One-way analysis of variance (ANOVA) followed by FDR post hoc multiple comparison test was performed for comparison among the groups.

Learning and memory
Morris water maze (MWM) test
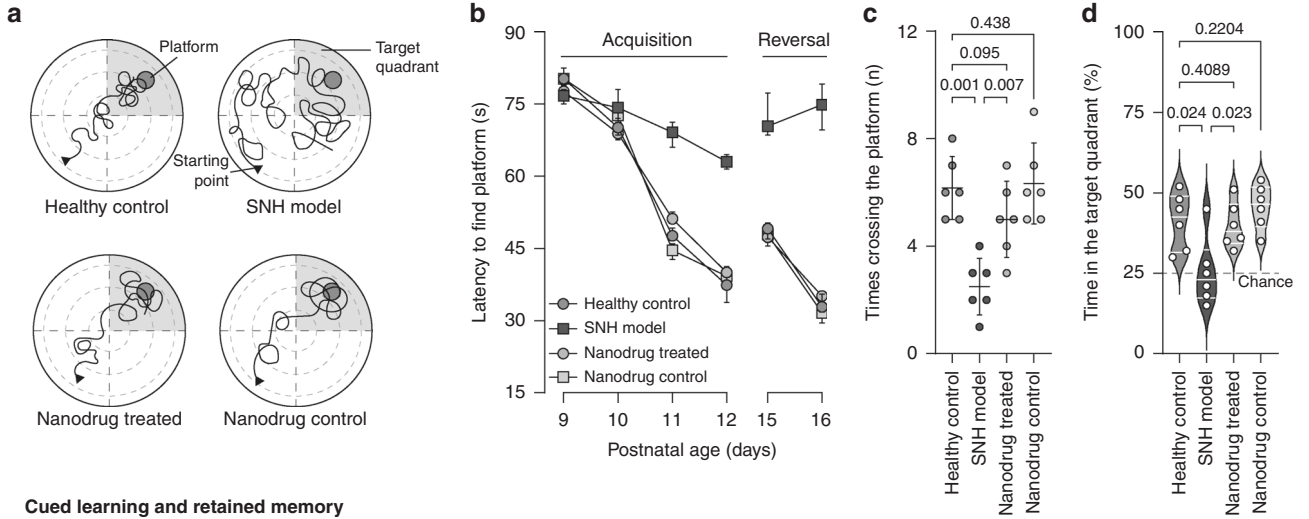
Cued learning and retained memory
Heading error in platform reversal MWM test
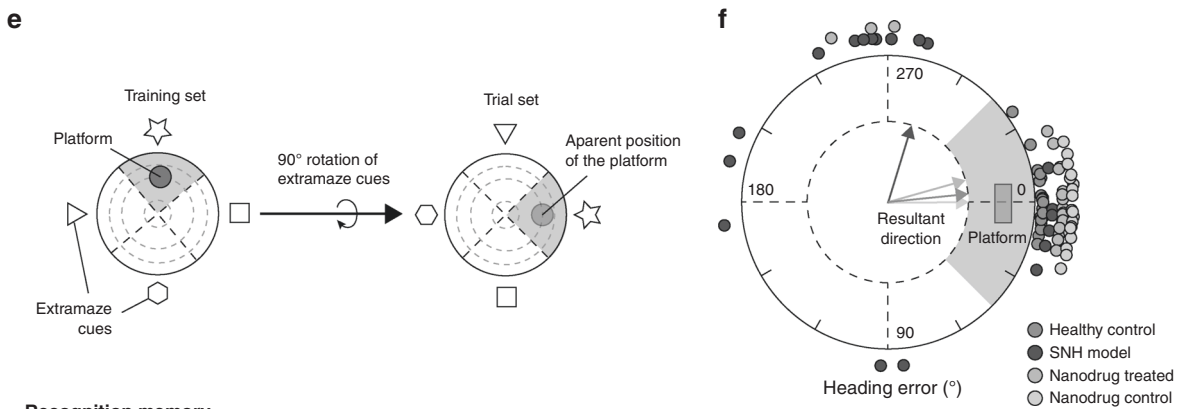
Recognition memory
Novel object recognition (NOR) test
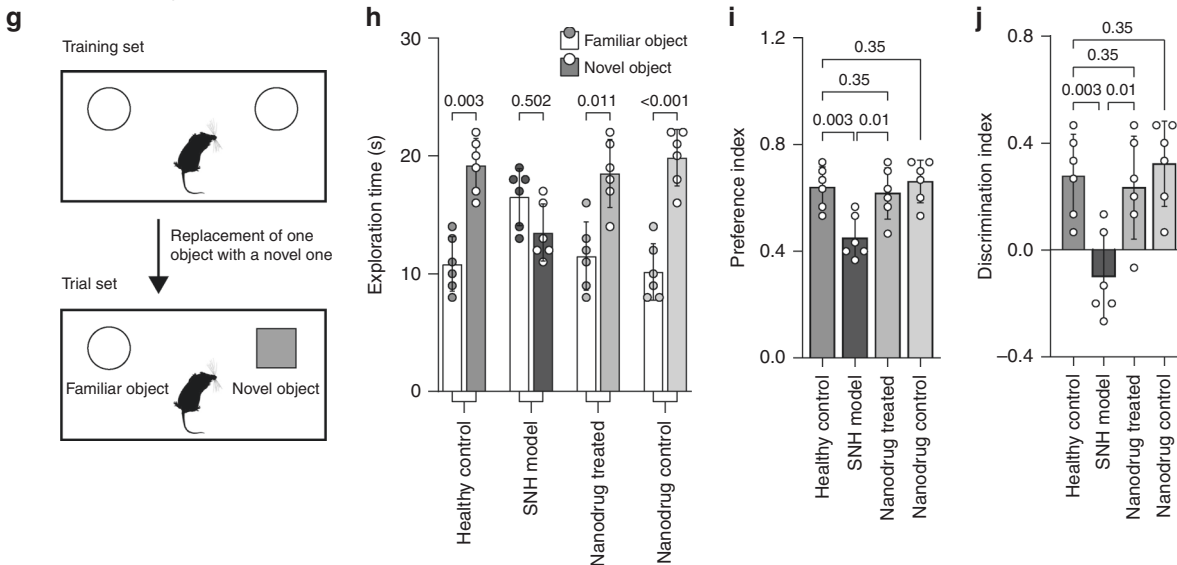
dependent recall memory and learning. Histopathological studies indicated that the nanodrug prevented neural cell injury in cerebellar, Purkinje, and substantia nigra region. In addition, the study drug ameliorated spongiosis, cell shrinkage, and eosinophilic neurons as observed in SNH brain parenchyma. Bilirubin-mediated oxidative damages in the brain as indicated by high GSH content, increased lipid peroxidation and low GSH:GSSH ratio, and decreased catalytic activities of antioxidant enzymes (i.e., CAT, GPx) in SNH model were

Fig. 5 **"Long-term" effects in learning and memory. a–d** Different parameters associated with Morris water maze (MWM) test. The SNH-BIND model showed difficulties in hippocampus-dependent learning. **e, f** Platform reversal MWM test for assessment of cued learning and retained memory. The SNH-BIND group did not follow the cues or retained memory resulting in greater heading errors. **g–j** Recognition memory as tested using novel object recognition (NOR) task. The SNH-BIND group was unable to recognize the novel object resulting in lower preference index for the novel object and lower discrimination index. In bar plots, data are expressed as mean ± SD ($n = 6$). Violins depict kernel density estimation of the underlying data distribution. Three lines (from the bottom to the top) in each violin plot show the location of the lower quartile (25th), the median, and the upper quartile (75th), respectively. Individual data points are represented as colored circles or squares ($n = 10$). Individual data points are represented as white circles ($n = 10$). One-way analysis of variance (ANOVA) followed by FDR post hoc multiple comparison test was performed for comparison among the groups.

reversed in nanodrug-treated cohort. The PK-PD studies indicate a therapeutic window that is almost immediate and sustainable. Within 24 h, the nanodrug is completely excreted through the fecal gastrointestinal route.

Our current data corroborate previous in vitro studies[23,40,50,51] that elucidated the direct destruction of bilirubin by the nanodrug to methyl-vinyl-maleimide. UV-visible spectroscopy, time-correlated single-photon counting, and electrochemical studies revealed the complex mechanism of bilirubin breakdown involving both surface catalysis (Langmuir–Hinshelwood type) and transient free radical-mediated charge transfer.[51] The origin of these catalytic mechanisms lies in the unique electronic structure of the nanodrug having closely packed tetrahedral and octahedral sites within a face-centered cubic oxygen framework. The valence band of the structure is dominated by tetrahedral Mn^{2+}, while the octahedral Mn-ions are in a Jahn-Tellar distorted, high-spin Mn^{3+} state.[23,48,52] The high-energy tetrahedral Mn^{2+} spontaneously oxidizes to Mn^{3+}, followed by the removal of electron from octahedral site, forming Mn^{4+}. When three electrons per formula unit are removed, the valence band becomes dominated by oxygen states and electrons are extracted from O2p orbitals instead of tetrahedral Mn^{3+}, resulting in the formation of oxygen holes on the nanodrug surface.[52] The holes degrade bilirubin by direct surface catalysis or creating transient free radicals upon interaction with dissolved molecular oxygen. While the reduction of bilirubin in the systemic circulation is clearly the result of direct interactions as described above (pharmacodynamics also shows a correlation between plasma nanodrug concentration and bilirubin degradation rate), the reduction of the brain bilirubin content may be both the consequence of the reduced blood content, as in phototherapy, as well as to a direct effect (degradation of bilirubin) operated by the nanodrugs that entered in the CNS. Our biodistribution study using ICP-AES further supports this argument by confirming the presence of nanodrug in the brain tissues. The amelioration of the brain oxidative damages could be a causal effect between reduction of brain bilirubin content and redox modulatory nature of the nanodrug. However, additional inquiries are needed to understand the complete molecular mechanism, which is beyond the scope of this article. It is worth mentioning here that, the free radicals generated during the breakdown process are transient and in absence of the inducer (i.e., bilirubin) are readily adsorbed by the nanodrug to replenish its initial electronic configuration.[39] Due to such redox buffering nature, the nanodrug showed neither cellular-toxicity nor damage to any bio-macromolecule.[24,25,53] A comprehensive repeated-dose sub-chronic (90 days) toxicity study[39] according to OECD guideline-408[54] further illustrated the biocompatibility and non-toxicity of this nanodrug in adult rodents.

At the outset, our data build the evidence of known properties of this manganese-based class of nanoparticles[55–57] as potential therapeutic agents. Our new results appear to confirm their crucial role in in vivo redox-mediated catalysis. We have demonstrated that these NPs do not possess discernible neurotoxic effects but appear to be neuroprotective. These findings are consistent with the previously reported amelioration of adult neuralgic conditions

like Mn-induced Parkinson's syndrome[26] and Huntington syndrome.[25]

Although the data are premature for immediate clinical trials, preparation of a comprehensive drug-safety-dossier including studies that would meet FDA endorsement could help overcome this problem. Prior commercial experiences to meet FDA approval have illustrated the limitations of establishing an effective collaboration of academia, industry, public health, regulatory and societal partners. Drug development strategies based on efficacy, safety, and affordability of an intervention are governed by its delivery as a wide-spread preventive, limited therapeutic, or a rare (orphan) application. Our preliminary report of this bilirubin degrading agent is a novel candidate for such a prospective inquiry.

The PHz-induced mice model is a widely used animal model for testing the efficacy of drugs against SNH but differs from human neonates who manifest increased bilirubin production and/or genetic mutation of bilirubin glucuronidation-related elimination. Our approach conducted the rodent studies at postnatal ages less than 14 days to avoid the developmental interference of bilirubin glucuronidation.[6] The observed yellow discoloration of brain, and histopathological damages to the midbrain, cerebellum, especially Purkinje cells, and the hippocampus region are well-known hallmarks of kernicterus and its sequelae.[58,59] Thus, a potential limitation is whether a chemically induced rodent model of SNH could be improved by future validation studies in naturally occurring animal models of unconjugated hyperbilirubinemia that manifest hemolytic, elimination, or combined disorders of bilirubin loads. Together with increased bilirubin, the experimental SNH model used in this study also presents an increased Fe and CO production. This may better represent a neonate with Rh incompatibility or G6PD deficiency.[60] Thus, replicating the experiments with long-term follow-up studies in a model of spontaneous and "pure" hyperbilirubinemia (e.g., the Gunn rat) will be important to confirm the efficacy and safety before suggesting the treatment for clinical trials. In this regard, assessment of inflammation and associated immunogenic parameters would be crucial to evaluate long-term effects of the treatment. We deferred the question about possible interaction with phototherapy since most neonates with hyperbilirubinemia are treated with photon exposure. Whether this nanodrug could augment use or substitute the use phototherapy to reverse acute bilirubin neurotoxicity needs to be resolved prospectively. The road map to ascertain potential clinical application of any chemo-preventive agent has been well charted by series of laboratory and clinical studies undertaken for seeking FDA approval of heme-oxygenase inhibitors. We propose a similar deliberative investigational strategy for a drug that could prevent life-long kernicteric disabilities.

In conclusion, we introduce a novel chemo-preventive nanoceutical agent that selectively degrades bilirubin in vivo and possesses unique properties to reverse acute bilirubin neurotoxicity. We provide direct evidence for a single oral dose of functionalized Mn_3O_4 nanoparticles (C-Mn_3O_4 NPs, the nanodrug) that is therapeutically effective in a chemically induced unconjugated SNH rodent model. Future clinical therapeutic options for

A. Adhikari et al.
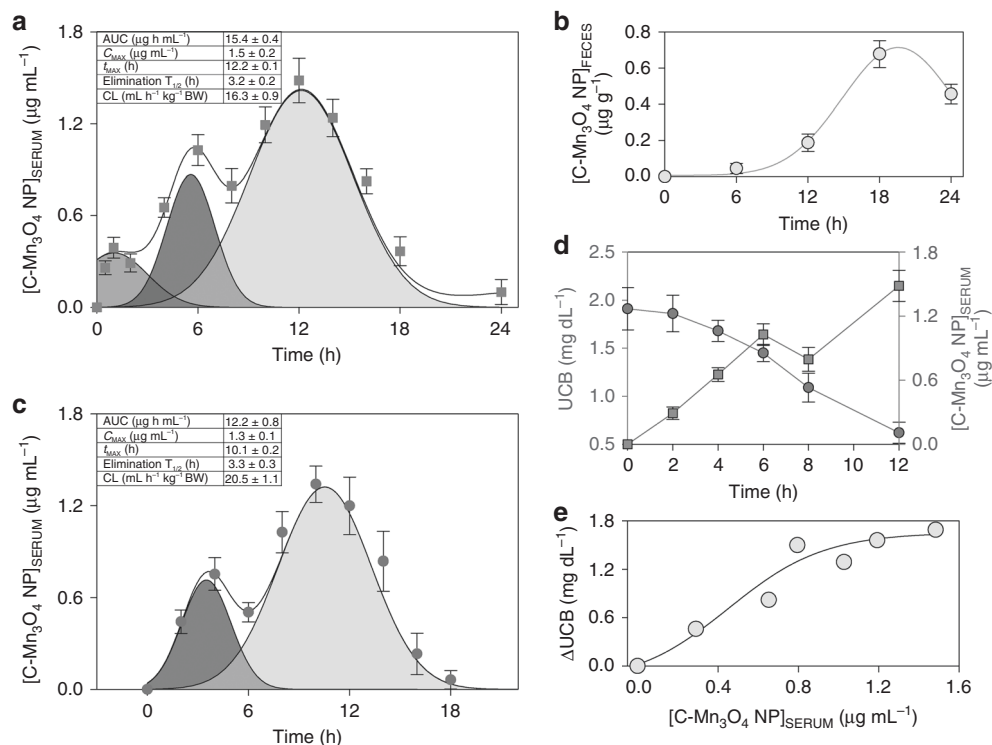
Fig. 6 Pharmacokinetics and pharmacodynamics of the nanodrug. a Plasma concentration-time profile following oral administration of the nanodrug. The inset table shows calculated pharmacokinetic parameters. **b** The elimination profile of C-Mn₃O₄ NPs through feces. **c** The plasma concentration-time profile of the nanodrug administered directly to the stomach. The inset table shows calculated pharmacokinetic parameters. **d** The change in UCB level and plasma nanodrug concentration with time. **e** Pharmacodynamics of bilirubin degradation. Data are expressed as mean ± SD ($n = 4$).

newborns at risk for incipient bilirubin neurotoxicity merit comprehensive inquiry and ascertainment to define public health benefits and individual risks.

DATA AVAILABILITY
All data that support the findings of this study are available within the published article. Study-related additional data will be available from S.K.P. upon legitimate request.

REFERENCES
1. Bhutani, V. K. & Stevenson, D. K. The need for technologies to prevent bilirubin-induced neurologic dysfunction syndrome. *Semin. Perinatol.* **35**, 97–100 (2011).
2. Slusher, T. M., Zipursky, A. & Bhutani, V. K. A global need for affordable neonatal jaundice technologies. *Semin. Perinatol.* **35**, 185–191 (2011).
3. Bhutani, V. K. et al. Clinical trial of tin mesoporphyrin to prevent neonatal hyperbilirubinemia. *J. Perinatol.* **36**, 533–539 (2016).
4. Qattea, I., Farghaly, M. A. A., Elgendy, M., Mohamed, M. A. & Aly, H. Neonatal hyperbilirubinemia and bilirubin neurotoxicity in hospitalized neonates: analysis of the US database. *Pediatr. Res.* (2021).
5. Olusanya, B. O., Teeple, S. & Kassebaum, N. J. The contribution of neonatal jaundice to global child mortality: findings from the GBD 2016 Study. *Pediatrics* **141**, e20171471 (2018).
6. Fujiwara, R., Nguyen, N., Chen, S. & Tukey, R. H. Developmental hyperbilirubinemia and CNS toxicity in mice humanized with the UDP glucuronosyltransferase 1 (UGT1) locus. *Proc. Natl Acad. Sci. USA* **107**, 5024 (2010).
7. Bhutani, V. K. et al. Neonatal hyperbilirubinemia and rhesus disease of the newborn: incidence and impairment estimates for 2010 at regional and global levels. *Pediatr. Res.* **74**, 86–100 (2013).
8. Dandona, R. et al. Subnational mapping of under-5 and neonatal mortality trends in India: The Global Burden of Disease Study 2000–17. *Lancet* **395**, 1640–1658 (2020).
9. Valaes, T., Petmezaki, S., Henschke, C., Drummond, G. S. & Kappas, A. Control of jaundice in preterm newborns by an inhibitor of bilirubin production: studies with tin-mesoporphyrin. *Pediatrics* **93**, 1–11 (1994).
10. Wong, R. J., Bhutani, V. K., Vreman, H. J. & Stevenson, D. K. Pharmacology review: tin mesoporphyrin for the prevention of severe neonatal hyperbilirubinemia. *NeoReviews* **8**, e77–e84 (2007).
11. Reddy, P., Najundaswamy, S., Mehta, R., Petrova, A. & Hegyi, T. Tin-mesoporphyrin in the treatment of severe hyperbilirubinemia in a very-low-birth-weight infant. *J. Perinatol.* **23**, 507–508 (2003).
12. Dennery, P. A. Metalloporphyrins for the treatment of neonatal jaundice. *Curr. Opin. Pediatr.* **17**, 167–169 (2005).
13. Drummond, G. S. & Kappas, A. Chemoprevention of severe neonatal hyperbilirubinemia. *Semin. Perinatol.* **28**, 365–368 (2004).
14. FDA Pediatric Advisory Committee. *FDA Advisory Committee Briefing Document: Stannsoporfin for the Treatment of Neonatal Hyperbilirubinemia* 1–162 (United States Food and Drug Administration (US-FDA), MD, USA, 2018).
15. Kinnear, C., Moore, T. L., Rodriguez-Lorenzo, L., Rothen-Rutishauser, B. & Petri-Fink, A. Form follows function: nanoparticle shape and its implications for nanomedicine. *Chem. Rev.* **117**, 11476–11521 (2017).
16. Pelaz, B. et al. Diverse applications of nanomedicine. *ACS Nano* **11**, 2313–2381 (2017).
17. Walkey, C. D. & Chan, W. C. W. Understanding and controlling the interaction of nanomaterials with proteins in a physiological environment. *Chem. Soc. Rev.* **41**, 2780–2799 (2012).
18. Wagner, V., Dullaart, A., Bock, A.-K. & Zweck, A. The emerging nanomedicine landscape. *Nat. Biotechnol.* **24**, 1211–1217 (2006).
19. Doshi, N. & Mitragotri, S. Designer biomaterials for nanomedicine. *Adv. Funct. Mater.* **19**, 3843–3854 (2009).
20. de Lázaro, I. & Mooney, D. J. Obstacles and opportunities in a forward vision for cancer nanomedicine. *Nat. Mater.* **20**, 1469–1479 (2021).
21. Barenholz, Y. C. In *Handbook of Harnessing Biomaterials in Nanomedicine* (ed. Peer, D.) 463–528 (Jenny Stanford Publishing, 2021).
22. United States Food and Drug Administration (US-FDA). *Drug Approval Package: Abraxane (Pcalitaxel Protein-Bound Particles) Injectable Suspension*. Accessed 12 Dec 2021. https://www.accessdata.fda.gov/drugsatfda_docs/nda/2005/21660_AbraxaneTOC.cfm (2005).
23. Adhikari, A., Polley, N., Darbar, S., Bagchi, D. & Pal, S. K. Citrate functionalized Mn₃O₄ in nanotherapy of hepatic fibrosis by oral administration. *Future Sci. OA* **2**, FSO146 (2016).

24. Adhikari, A. et al. Redox nanomedicine ameliorates chronic kidney disease (CKD) by mitochondrial reconditioning in mice. *Commun. Biol.* **4**, 1013 (2021).

25. Adhikari, A. et al. Incorporation of a biocompatible nanozyme in cellular anti-oxidant enzyme cascade reverses huntington's like disorder in preclinical model. *Adv. Healthc. Mater.* **10**, 2001736 (2021).

26. Adhikari, A. et al. Manganese neurotoxicity: nano-oxide compensates for ion-damage in mammals. *Biomater. Sci.* **7**, 4491–4502 (2019).

27. Xu, Z. et al. Facet-dependent biodegradable Mn_3O_4 nanoparticles for ameliorating Parkinson's disease. *Adv. Healthc. Mater.* **10**, 2101316 (2021).

28. Aschner, J. L. & Aschner, M. Nutritional aspects of manganese homeostasis. *Mol. Asp. Med.* **26**, 353–362 (2005).

29. Avila, D. S., Puntel, R. L. & Aschner, M. In *Metal Ions in Life Sciences* Vol. 13 (eds Sigel, A., Sigel, H. & Sigel, R. K. O.) 199–227 (Springer Netherlands, 2013).

30. Emsley, J. Manganese the protector. *Nat. Chem.* **5**, 978–978 (2013).

31. Mattison, D. R. et al. Severity scoring of manganese health effects for categorical regression. *NeuroToxicology* **58**, 203–216 (2017).

32. Li, L. & Yang, X. The essential element manganese, oxidative stress, and metabolic diseases: links and interactions. *Oxid. Med. Cell. Longev.* **2018**, 7580707 (2018).

33. Mondal, S. et al. Novel one pot synthesis and spectroscopic characterization of a folate-Mn_3O_4 nanohybrid for potential photodynamic therapeutic application. *RSC Adv.* **9**, 30216–30225 (2019).

34. Singh, N., Savanur, M. A., Srivastava, S., D'Silva, P. & Mugesh, G. A manganese oxide nanozyme prevents the oxidative damage of biomolecules without affecting the endogenous antioxidant system. *Nanoscale* **11**, 3855–3863 (2019).

35. Yao, J. et al. ROS scavenging Mn_3O_4 nanozymes for in vivo anti-inflammation. *Chem. Sci.* **9**, 2927–2933 (2018).

36. Huang, C.-C. et al. Chronic manganese intoxication. *Arch. Neurol.* **46**, 1104–1106 (1989).

37. Crossgrove, J. & Zheng, W. Manganese toxicity upon overexposure. *NMR Bio-medicine* **17**, 544–553 (2004).

38. Institute of Medicine (US) Panel on Micronutrients. *Dietary Reference Intakes for Vitamin A, Vitamine K, Arsenic, Boron, Chromium, Copper, Iodine, Iron, Manganese, Molybdenum, Nickel, Silicon, Vanadium, and Zinc.* 394–419 (Institute of Medicine (US) Washington DC, USA, 2001).

39. Adhikari, A. et al. Redox buffering capacity of nanomaterials as an index of ROS-based therapeutics and toxicity: a preclinical animal study. *ACS Biomater. Sci. Eng.* **7**, 2475–2484 (2021).

40. Giri, A. et al. Unprecedented catalytic activity of Mn_3O_4 nanoparticles: potential lead of a sustainable therapeutic agent for hyperbilirubinemia. *RSC Adv.* **4**, 5075–5079 (2014).

41. Rice, A. C. & Shapiro, S. M. A new animal model of hemolytic hyperbilirubinemia-induced bilirubin encephalopathy (kernicterus). *Pediatr. Res.* **64**, 265–269 (2008).

42. Amini, N. et al. Animal kernicterus models: progress and challenges. *Brain Res.* **1770**, 147624 (2021).

43. Bortolussi, G. & Muro, A. F. Experimental models assessing bilirubin neurotoxicity. *Pediatr. Res.* **87**, 17–25 (2020).

44. Maity, S., Nag, N., Chatterjee, S., Adhikari, S. & Mazumder, S. Bilirubin clearance and antioxidant activities of ethanol extract of phyllanthus amarus root in phenylhydrazine-induced neonatal jaundice in mice. *J. Physiol. Biochem.* **69**, 467–476 (2013).

45. Chen, S. & Tukey, R. H. Humanized UGT1 mice, regulation of UGT1A1, and the role of the intestinal tract in neonatal hyperbilirubinemia and breast milk-induced jaundice. *Drug Metab. Disposition* **46**, 1745 (2018).

46. Yueh, M.-F., Chen, S., Nguyen, N. & Tukey, R. H. Developmemntal onset of bilirubin-induced neurotoxicity involves toll-like receptor-2 dependent signalling in humanized UDP-glucuronosyltransferase1 mice. *J. Biol. Chem.* **289**, 4699–4709 (2014).

47. Buege, J. A. & Aust, S. D. In *Methods in Enzymology* Vol. 52 (eds Fleischer, S. & Packer, L.) 302–310 (Academic Press, 1978).

48. Adhikari, A. et al. A smart nanotherapeutic agent for in vitro and in vivo reversal of heavy-metal-induced causality: key information from optical spectroscopy. *ChemMedChem* **15**, 420–429 (2020).

49. Benjamini, Y., Krieger, A. M. & Yekutieli, D. Adaptive linear step-up procedures that control the false discovery rate. *Biometrika* **93**, 491–507 (2006).

50. Adhikari, A., Mondal, S., Darbar, S. & Kumar Pal, S. Role of nanomedicine in redox mediated healing at molecular level. *Biomolecular Concepts* **10**, 160–174 (2019).

51. Mondal, S. et al. Interaction of a jaundice marker molecule with a redox-modulatory nano-hybrid: a combined electrochemical and spectroscopic study toward the development of a theranostic tool. *ChemMedChem* e202100660 (2022).

52. Morgan Chan, Z. et al. Electrochemical trapping of metastable Mn^{3+} ions for activation of MnO_2 oxygen evolution catalysts. *Proc. Natl Acad. Sci. USA* **115**, E5261–E5268 (2018).

53. Polley, N. et al. Safe and symptomatic medicinal use of surface-functionalized Mn_3O_4 nanoparticles for hyperbilirubinemia treatment in mice. *Nanomedicine* **10**, 2349–2363 (2015).

54. Organisation for Economic Co-operation and Development (OECD). *Test No. 408: Repeated Dose 90-Day Oral Toxicity Study in Rodents* (2018).

55. Lei, S., Tang, K., Fang, Z. & Zheng, H. Ultrasonic-assisted synthesis of colloidal Mn_3O_4 nanoparticles at normal temperature and pressure. *Cryst. Growth Des.* **6**, 1757–1760 (2006).

56. Pike, J., Hanson, J., Zhang, L. & Chan, S.-W. Synthesis and redox behavior of nanocrystalline (Mn_3O_4). *Chem. Mater.* **19**, 5609–5616 (2007).

57. Gagrani, A., Ding, B., Wang, Y. & Tsuzuki, T. pH dependent catalytic redox properties of Mn_3O_4 nanoparticles. *Mater. Chem. Phys.* **231**, 41–47 (2019).

58. Shapiro, S. M. Definition of the clinical spectrum of kernicterus and bilirubin-induced neurologic dysfunction (bind). *J. Perinatol.* **25**, 54–59 (2005).

59. Cayabyab, R. & Ramanathan, R. High unbound bilirubin for age: a neurotoxin with major effects on the developing brain. *Pediatr. Res.* **85**, 183–190 (2019).

60. Francis, R. O. et al. Glucose-6-phosphate dehydrogenase deficiency in transfusion medicine: the unknown risks. *Vox Sanguinis* **105**, 271–282 (2013).

AUTHOR CONTRIBUTIONS

A.A., V.K.B., A.K.M and S.K.P. conceived and planned the study. A.A., S.M., M.D., N.P., and S.D. performed animal experiments and biochemical studies. A.A. executed numerical calculations and statistical analysis. A.A., S.D., S.S.B., D.P., A.K.M., V.K.B, and S.K.P. contributed to the interpretation of the results. A.K.D. carried out and evaluated the histological studies. A.A. and V.K.B. took the lead in writing the manuscript. All authors provided critical feedback and helped in shaping the research, analysis, interpretation, and writing. All authors reviewed, edited, and approved the final version of the manuscript.

COMPETING INTERESTS

The authors declare no competing interests.

ETHICS APPROVAL AND CONSENT TO PARTICIPATE

This study does not involve human subject or clinical study. Thus, patient consent was not required. All animal studies and experimental procedures were performed at Central Animal Facility, Department of Zoology, Uluberia College, India (Reg. No.: 2057/GO/ReRcBi/S/19/CPCSEA) following the protocol approved by the Institutional Animal Ethics Committee (Ref: 02/S/UC-IAEC/01/2019) as per standard guideline of Committee for the Purpose of Control and Supervision of Experiments on Animals (CPCSEA), Govt. of India.

ADDITIONAL INFORMATION

Supplementary information The online version contains supplementary material available at https://doi.org/10.1038/s41390-022-02179-5.

Correspondence and requests for materials should be addressed to Samir Kumar Pal.

Reprints and permission information is available at http://www.nature.com/reprints

Publisher's note Springer Nature remains neutral with regard to jurisdictional claims in published maps and institutional affiliations.